Published in final edited form as:
Dev Biol. 2005 July 1; 283(1): 140–156.

Dosage-dependent requirement for mouse *Vezf1* in vascular system development

Frank Kuhnert[a,b,1], **Luisa Campagnolo**[a,2,3], **Jing-Wei Xiong**[b,2,4], **Derek Lemons**[a], **Michael J. Fitch**[a], **Zhongmin Zou**[a], **William B. Kiosses**[a], **Humphrey Gardner**[a,5], and **Heidi Stuhlmann**[a,b,*]

a*Department of Cell Biology, Division of Vascular Biology, Mail CVN-26, The Scripps Research Institute, 10550 North Torrey Pines Road, La Jolla, CA 92037, USA*

b*Department of Biochemistry and Molecular Biology, Mount Sinai School of Medicine, New York, NY 10029, USA*

Abstract

Vezf1 is an early development gene that encodes a zinc finger transcription factor. In the developing embryo, Vezf1 is expressed in the yolk sac mesoderm and the endothelium of the developing vasculature and, in addition, in mesodermal and neuronal tissues. Targeted inactivation of Vezf1 in mice reveals that it acts in a closely regulated, dose-dependent fashion on the development of the blood vascular and lymphatic system. Homozygous mutant embryos display vascular remodeling defects and loss of vascular integrity leading to localized hemorrhaging. Ultrastructural analysis shows defective endothelial cell adhesion and tight junction formation in the mutant vessels. Moreover, in heterozygous embryos, haploinsufficiency is observed that is characterized by lymphatic hypervascularization associated with hemorrhaging and edema in the jugular region; a phenotype reminiscent of the human congenital lymphatic malformation syndrome cystic hygroma.

Keywords

Vezf1 function; ES cells; Knockout mice; Endothelial cells; Vascular development; Angiogenesis; Lymphangiogenesis

Introduction

Mammals have two structurally different circulatory systems, the closed blood vasculature and the open lymphatic system, that are functionally connected and act in concert to maintain tissue homeostasis. The blood vascular system, consisting of arteries, capillaries, and veins, efficiently carries nutrients, gases, and waste products to and from distant actively metabolizing tissues. The lymphatic system regulates tissue fluid balance by returning interstitial fluid and macromolecules from the tissue spaces of most organs back into the venous circulation and serves as a conduit for trafficking immune cells, thus complementing the function of the blood vascular system.

*Corresponding author. Department of Cell Biology, Division of Vascular Biology, Mail CVN-26, The Scripps Research Institute, 10550 North Torrey Pines Road, La Jolla, CA 92037, USA. Fax: +1 858 783 7374. E-mail address: hstuhlm@scripps.edu (H. Stuhlmann).
[1]Present address: Department of Medicine, Division of Hematology, Stanford University Medical Center, Stanford, CA 94305, USA.
[2]These authors contributed equally to the manuscript.
[3]Present address: Dip.to Sanita Pubblica e Biologica Cellulare, Universita degli studi di Roma “Tor Vergata”, Italy.
[4]Present address: Cardiovascular Research Center, Massachusetts General Hospital-East, Charlestown, MA 02129, USA.
[5]Present address: Biogen Inc., Cambridge, MA 02142, USA.

During embryonic development, the blood vascular system is formed via two distinct processes. Vasculogenesis describes the initial differentiation of mesodermally derived endothelial precursor cells, angioblasts, and their coalescence into a primitive vascular network. Angiogenesis refers to the subsequent growth, remodeling, and maturation processes of the primary vascular plexus to give rise to the mature blood vasculature (Carmeliet, 2000; Risau, 1997). The lymphatic system develops through sprouting from the venous system, a process that becomes first apparent in the jugular region of developing embryos at midgestation (Wigle and Oliver, 1999).

The vascular endothelial growth factor (VEGF) signaling pathway plays a critical role in the regulation of both blood vascular and lymphatic development. VEGF-A signaling, through binding to its blood endothelial cell-specific receptors VEGFR-1 and VEGFR-2, is essential for the early stages of blood vascular development and the initiation of vascular sprouting (Carmeliet et al., 1996a; Ferrara et al., 1996). In contrast, selective activation of VEGFR-3 signaling using receptor-specific mutants of VEGF-C and VEGF-D induces lymphangiogenesis in the skin of transgenic mice (Veikkola et al., 2001). The importance of VEGFR-3 signaling for lymphatic development is underscored by the findings that lymphatic vessels in VegfC-null embryos fail to sprout (Karkkainen et al., 2004), overexpression of soluble VEGFR-3 leads to inhibition of lymphangiogenesis (Makinen et al., 2001), and mutations in the tyrosine kinase domain of VEGFR-3 are linked to human hereditary primary lymphedema (Karkkainen et al., 2000). Recently, angiopoietin signaling, in addition to its well-established function during blood vascular remodeling and vessel stabilization (Gale and Yancopoulos, 1999), has also been implicated in the regulation of lymphatic development (Gale et al., 2002).

At the level of transcriptional regulation, Prox1 activity is required for maintaining lymphatic endothelial cell sprouting, and loss of Prox1 function results in arrested lymphatic development without affecting blood vessel formation (Wigle et al., 1999,2002). Moreover, misexpression of Prox1 in blood endothelial cells confers a lymphatic endothelial phenotype, indicating that Prox1 is a master regulator of the lymphatic endothelial cell fate (Hong et al., 2002;Petrova et al., 2002). Using gene inactivation approaches, several transcription factors have been implicated in blood vascular development (for review, see Oettgen, 2001). For instance, genetic ablation of the bHLH-PAS protein hypoxia inducible factor 1α (HIF-1α) leads to defective yolk sac and cephalic vascularization (Iyer et al., 1998;Ryan et al., 1998), while the zinc finger lung Krüppel-like factor (LKLF) is required for vascular smooth muscle cell and pericyte recruitment during vessel stabilization (Kuo et al., 1997).

Vascular endothelial zinc finger 1 (Vezf1) was originally identified as a gene specifically expressed in vascular endothelial cells during early embryonic development (Xiong et al., 1999), although our subsequent analysis indicated expression in mesodermal and neuronal tissues as well (Lemons et al., 2005). Vezf1 encodes a 518 amino acid nuclear protein that contains six zinc finger motifs of the C2H2 (Krüppel-like)-type and a proline-rich transcriptional transactivation domain at its C-terminus (Lemons et al., 2005). Consistent with the hypothesis that VEZF1 is a bona fide transcription factor, the human ortholog ZNF161/DB1 has been shown to selectively transactivate the endothelial cell-specific human endothelin-1 promoter in vitro (Aitsebaomo et al., 2001). In addition, Vezf1 has been implicated in the regulation of endothelial cell proliferation, migration, and network formation in vitro (Miyashita et al., 2004). To investigate the role of Vezf1 in vivo, we have generated a null allele by gene targeting. Here we report that inactivation of Vezf1 results in lethality caused by angiogenic remodeling defects and loss of vascular integrity in homozygous mutant embryos. Furthermore, loss of a single Vezf1 allele leads to an incompletely penetrant phenotype characterized by lymphatic hypervascularization that is associated with hemorrhaging and edema in the jugular region. This haploinsufficient phenotype is reminiscent

of the human congenital malformation syndrome, cystic hygroma (Gallagher et al., 1999). Our studies show that Vezf1 is a crucial regulator of blood vessel and lymphatic development that acts in a tightly regulated dose-dependent fashion during embryonic development.

Materials and methods

Construction of the Vezf1 targeting construct and ES cell manipulations

A 5′ Vezf1 cDNA fragment (nt 3–776 of the published mouse Vezf1 cDNA sequence, GenBank accession no. AF104410; Xiong et al., 1999) was used as a probe to screen a mouse 129/Sv lambda genomic library (provided by K. Andrikopoulous and F. Ramirez, Mount Sinai School of Medicine). One positive phage clone contained the first and second exon separated by 5 kb of intronic sequence and 15 kb of genomic sequence upstream of exon 1. For construction of the targeting vector, an 8-kb EcoRV/XhoI fragment containing the first exon, 6 kb of upstream genomic sequences and 2 kb of 3′ intronic sequence, was subcloned into pBluescriptIISK (Stratagene). A 390-bp EagI fragment including the ATG translation initiation codon was replaced with an IRES-lacZgt1.2neo cassette (Wang and Lufkin, 2000) via NotI linkers. Subsequent analysis of the Vezf1 promoter revealed that the deletion included 91 bp upstream of the transcriptional start site, resulting in a non-functional lacZ allele.

R1 ES cells (Nagy and Rossant, 1993) were maintained in DMEM (high glucose) containing 15% heat-inactivated fetal calf serum (FCS), 0.1 mM h-mercaptoethanol, 20 mM HEPES, pH 7.3, 0.1 mM non-essential amino acids, and 1000 U/ml LIF on g-irradiated primary MEFs as a feeder layer. The targeting vector was linearized with XhoI and introduced into R1 cells by electroporation (400 V, 125 AF; Bio-Rad Gene Pulser). ES cell clones were selected at G418 concentrations of 200–350 Ag/ml for 10 days. ES cell clones homozygous for the targeted Vezf1 allele were obtained by hyperselection (Mortensen et al., 1992) at concentrations between 400 and 1000 Ag/ml of G418 for 14 days. Three independent clones with correctly targeted alleles (V2, V74, V86) were identified by Southern blot analysis of BamHI-digested genomic DNA using a [a-^{32}P]-dCTP-labeled 5′ genomic fragment (EcoRV–EcoRV fragment of 1-kb length) and a 3′ cDNA fragment corresponding to the second exon (BamHI–PstI of 500-bp length) as probes. ES cells were induced to differentiate in suspension cultures into embryoid bodies as described previously (Leahy et al., 1999).

Northern analysis

Total RNA was prepared from ES cells and embryoid bodies using a RNeasy Mini Kit (Qiagen). RNA (10 Ag each) was analyzed on Northern blots as described (Xiong et al., 1999) using a [a-^{32}P]-dCTP-labeled Vezf1 cDNA fragment (nucleotides 3–776) as a probe. To control for RNA loading, filters were stripped and hybridized with [a-^{32}P]-dCTP-labeled mouse GAPDH cDNA plasmid.

Generation of Vezf1 KO mice and genotyping

Chimeric mice were generated by injection of *Vezf1*$^{+/-}$ ES cells from clones V2, V74, and V86 into C57BL/6 blastocysts (performed by the Transgenic Core Facility at Mount Sinai School of Medicine). Mice at weaning age and staged embryos from E14.5 to birth (the morning of the vaginal plug was counted as day 0.5 post-coitum) were genotyped by Southern blot analysis of BamHI-digested tail or yolk sac DNA, respectively. A 500-bp fragment from exon 2 was used as a 3′ flanking probe for Southern blot analysis (see above). Staged embryos from E8.5 to E13.5 were genotyped by genomic PCR. Primers for the wild type Vezf1 allele are: 5′ (5′-GCGTCCCGGAGGTTACCGAA-GTGG-3′) and 3′ (5′-GGAACAGGAACGCGGTCCAGTTGG-3′), yielding an amplification product of 150 bp; primers for the targeted allele are: 5′ (5′-TTTCTCTGGGCCGCGGGGTGGT-3′) and 3′ (5′-GCGGGGATCTCATGCTGGAGTT-3′), yielding a 300-bp amplification product.

Western blot analysis and antibodies

E12.5 embryos from heterozygous intercrosses were homogenized in 500 Al RIPA buffer each. 40-Ag samples of denatured protein were resolved on 10% SDS gels and transferred to polyvinylidene difluoride (PVDF) membranes (Millipore Corporation, Bedford, MA) using standard procedures. Anti-VEZF antibody against the N-terminal peptide AIGIKKEKPKTSFV (1 Ag/ml, Multiple Peptide Systems, San Diego; Lemons et al., 2005) and horseradish peroxidase-conjugated anti-rabbit IgG (Amersham Biosciences, Piscataway, NJ) were used. Specific bands were detected with ECL Plus Western Blot Reagent (Amersham). To control for loading, blots were stripped and reprobed with anti-h-tubulin antibody (1:2000 dilution).

Whole-mount PECAM-1 staining of embryos and yolk sacs

Staged embryos from the fifth backcross generation (F5) were fixed in 4% paraformaldehyde (PFA)/PBS overnight at +4°C, dehydrated through a methanol series, and stored in 100% methanol at -20°C. Embryos were bleached in 6% hydrogen peroxide/methanol for 1 h at room temperature and rehydrated through a methanol series to PBS/0.1% Tween 20 (PBST). After blocking in 3% instant skim milk/PBST (PBSMT) twice for 1 h, the embryos were incubated overnight at +4°C with a monoclonal rat anti-mouse CD31 (PECAM-1) antibody (1:50 dilution in PBMST; MEC13.3, Pharmingen) (Krebs et al., 2000). Embryos were washed with PBSMT five times for 1 h at +4°C and incubated with peroxidase-conjugated donkey anti-rat secondary antibody (Jackson Immunoresearch) overnight at +4°C in PBST. Peroxidase reaction was visualized with DAB/hydrogen peroxide. Yolk sacs were embedded in paraffin, thin-sectioned, and counterstained with Nuclear Fast Red.

Histology and immunohistochemistry

Litters from timed ($Vezf1^{+/-} \times Vezf1^{+/-}$) matings were recovered between E8.5 and birth. Yolk sacs were isolated for genotyping and embryos were photographed in ice-cold PBS under a Nikon SMZ-U stereomicroscope with a 35-mm camera. After overnight fixation in 4% PFA/PBS at +4°C, the embryos were dehydrated and embedded in paraffin. Serial sections (5 Am) were deparaffinized, rehydrated, and stained with hematoxylin and eosin (H&E). Immunohistochemistry on paraffin sections of embryos was performed according to standard protocols. The following antibodies were used: mouse anti-SMa-actin/HRP (DAKO, 1:100), rat anti-PECAM-1 (BD Pharmingen, 1:100), rat anti-mouse VEGFR-3 (kindly provided by H. Kubo and K. Alitalo) (Kubo et al., 2000), rabbit anti-mouse LYVE-1 antibody (kindly provided by D. Jackson) (Prevo et al., 2001). All antibody-stained sections were counterstained with hematoxylin. Photomicrographs were taken under a Zeiss Axioplan2 microscope with a digital Zeiss AxioCam color camera.

For immunofluorescence studies, the following antibodies were used: rabbit anti-Prox1 (1:100 dilution; kindly provided by G. Oliver), rat anti-mouse CD31 (1:200; BD Pharmingen), rabbit anti-collagen IV (1:200; Chemicon), rabbit anti-ZO-1 (1:100; Zymed), and rat anti-mouse VE-cadherin (1:20; BD Pharmingen). Staged embryos were fixed overnight at 4°C in 4% PFA/PBS, cryoprotected in 30% sucrose/PBS, and embedded in OCT (TissueTek). Ten-micron cryostat sections were stained according to standard protocols. Primary antibodies were incubated overnight at 4°C, and staining was revealed with Alexa488-labelled rabbit anti-rat IgG and Cy3-labelled goat anti-rabbit IgG, respectively. Control sections were incubated with nonspecific rabbit and rat IgG using conditions as described above. Slides were mounted with fluorescent mounting medium (DAKO), examined under an epifluorescence (Zeiss Axioplan2) or under a confocal microscope (Bio-Rad MRC-1024), respectively, and photographed.

Transmission electron microscopy

Heads of E9.5 embryos were placed overnight in ice-cold fixative (4% paraformaldehyde, 1.5% glutaraldehyde in 0.1 M Na cacodylate buffer). Preparation of samples and analysis by electron microscopy were performed by the Microscopy Core Facility at The Scripps Research Institute. Following standard procedures, specimens were examined under a Philips CM100 electron microscope (FEI, Hillsbrough OR), and images were documented using Kodak SO163 EM film.

Vessel morphometry

PECAM-1-stained sections of E13.5 wild type and heterozygous mutant embryos were counterstained with hematoxylin. Quantitative morphometric analysis was performed essentially as described (Pozzi et al., 2000). Briefly, sections were imaged with a digital camera (Pixera, Los Gatos, CA). Images were processed by using Scion Image software (Frederick, MD). PECAM-1-positive structures in the neck region of embryos were automatically counted, and their area was measured (values represent area occupied by PECAM-1 positive structures per microscopic field, expressed in percent). Differences in vascularity (number of and area occupied by PECAM-1-positive structures per embryo microscopic field) were determined for each section. A total of 3 heterozygous mutant and wild type embryos each were analyzed.

Cultivation of megakaryocytes from embryonic livers

Fetal livers from E12.5 embryos were isolated and placed into low-glucose DMEM supplemented with 10% FCS and 10 ng/ml mouse TPO (Lecine et al., 1998). Liver cells were dissociated by drawing them subsequently through 20-g and 25-g needles. Cells from one liver were seeded into a 6-well dish and incubated at 37°C in 5% CO_2. After 6 days of culture, cells were visually examined under the microscope, harvested, and stained with Wright–Giemsa solution.

Gene expression analysis

Total RNA was isolated from E10.5 embryos using Trizol (Life Technologies) and treated with DNaseI (Life Technologies) according to the manufacturer's instructions. Total RNA (2 Ag) was reverse transcribed using random hexamers with the Superscript First Strand Synthesis System (Life Technologies) according to the manufacturer's instructions. PCR was performed using 1 Al of the reverse transcriptase reaction in a volume of 50-Al using Hotstar Taq polymerase (Qiagen). The PCR conditions were as follows: initial denaturation at 95°C for 10 min followed by up to 35 cycles of denaturation at 95°C (1 min), annealing at 58°C (1 min), and extension at 72°C (1 min). 5-Al aliquots were taken after 25, 30, and 35 cycles and amplified PCR products were analyzed by electrophoresis on a 2% agarose gel. PCR primer pairs were as follows: Flk-1: 5′-TCTGTGGTTCTGCGTGGAGA-3′, 5′-GTATCATTTCC-AACCACCCT-3′; Flt-1: 5′-TGT-GGAGAAACTTG-GTGACCT-3′, 5′-TGGAGAACAGCAGGACTCCTT-3′; Flt-4: 5′-CACCGAAGC-AGACGCTGATGAT-3′, 5′-AGCTGCTGTCTGCGAAGAAG-3′; VEGF-A: 5′-GTAACGATG-AAGCCCTGGAGTG-3′, 5′-TGA-GAGGTCTGGTTCCCGAAAC-3′; VEGF-C: 5′-AA-ATGTACA-AGTGCCAGCTGCGGAA-3 V, 5 V-GGCATCGGCACATGTAGTTATTCCA-3′; VEGF-D: 5 V-ACGA-TCTGAACAACAGATCCGAGCA-3 V, 5′-TCTGGGGTCTGAATGGATCTTCTGA-3′; Tie1: 5′-TC-TTTGCTGCTCCCCACTCT-3′, 5′-ACACACCAT-TCGCCATCAT-3′; Tie2: 5′-CCTTCCTAC-CTG-CTACTTTA-3′,5′-CCACTACACCTTTCTTTACA-3′; Ang1:5′-AAGGGAGGAAAAAGAGA-AGAA-GAG-3 V,5 V-GTTAGCATGA-GAGCGCATTTG-3 V; Ang2: 5′-TGCCTACACTACCAGA-AGAAC-3′, 5′-T-ATTTACTGCTGAACTCCCAC-3 V; Notch1: 5 V-TGCCTGAATGGAGGTAG-GTGCGAA-3′, 5′-G-CACAGCGATAGGAGCCGATCTCA-3′; Notch4: 5′-

CCAAGAGATTCCCTT-AAACTCGG-3′, 5′-CCAGA-GTTTAGGGATTCTCG-3′; Dll4: 5′-GACTGAGCTACTC-TTAC-CGGGTCA-3′, 5′-CTTACAGCTGCCACCATTTC-GACA-3 V; EphrinB2:5 V-CTGTGCCAGACCAG-ACCAAGA-3′,5′-CAGCAGAACTTGCATCTTGTC-3′; EphB4: 5′-CAGGTGGTCAGCGCTC-TGGAC-3′,5′-ATCTGCCACGGTGGTGAGTC-3′; Prox-1: 5′-TTT-CAATGCCATCATCGCG-GGCAAAG-3′, 5′-TCACGTG-CACTTTACACAGGCTGACA-3′; podoplanin: 5′-AC-CCTGGTTGG-AATCATAGTTGGCGT-3 V,5 V-AG-GGTGAACCCATGGTTACAGTTGCT-3′;Tbx1:5′-GTTGCAG-CCTTCGCAGCCAGCA-3′, 5′-TAGT-GTACTCGGCCAGGTGTAGCA-3′; LKLF: 5′-CCAC-ACATA-CTTGCAGCTACAC-3′,5′-CCATCGTCTCCC-TTATAGAAATA-3 V; EDG-1: 5 V-TAGCAGCTA-TGGTGTCCACTAG-3′, 5′-GATCCTGCAGTAGAG-GATGGC-3′; Endoglin: 5′-TACTCATGTCC-CTGATC-CAGCC-3′,5′-GTCGATGCACTGTACCTTTTTCC-3′; VE-cadherin: 5′-GG-ATGCAGA-GGCTCACA-GAG-3′, 5′-CTGGCGGTTCACGTTGGACT-3′; ET-1: 5′-TGTCTT-GGGAGCCG-AACTCA-3′,5′-GC-TCGGTTGTGCGTCAACTTCTGG-3′; Vezf1: 5′-GTCTCATGAAGGAGGCA-TCACCA-3′, 5′-ACATG-TTTTACATGACAGCTTAGGT-3′; b-actin:5′-GTG-GGCCGCTCTAGG-CACCAA-3′,5′-CTCTTTGATGT-CACGCACGATTTC-3′.

Results

Targeted disruption of the Vezf1 gene in mouse embryonic stem cells

A 20-kb genomic Vezf1 fragment was isolated that contained the first and second coding exons of 153- and 695-bp length, respectively, the first intron of 5-kb length, and 15 kb of genomic sequence upstream of exon 1. A targeting vector was constructed that replaced exon 1 and the proximal part of the first intron with a promoter-less IRES-lacZ gene and a neo expression cassette (Fig. 1A). The construct was introduced into R1 ES cells, and three independent clones out of 96 G418-resistant clones analyzed contained the correctly targeted allele (Fig. 1B). An ES cell clone that carried the introduced mutation in both alleles (Fig. 1C) was obtained by G418 hyperselection (Mortensen et al., 1992). Using a probe corresponding to the second coding exon, low levels of Vezf1 transcripts were detected by Northern analysis in undifferentiated wild type R1 cells, and high levels in day 6 embryoid bodies derived from wild type R1 cells (Fig. 1D), consistent with previous studies (Xiong et al., 1999). In contrast, Vezf1 mRNA was reduced by about half in embryoid bodies derived from heterozygous ES cells and was absent in undifferentiated *Vezf1*$^{-/-}$ ES cells or in embryoid bodies derived from this clone (Fig. 1D). Furthermore, Vezf1 mRNA could not be detected in KO embryos by RT-PCR using primer pairs spanning the entire coding sequence (data not shown), indicating that the targeting event resulted in a null mutation. Consistent with this, VEZF1 protein expression was reduced in heterozygous, and undetectable in homozygous mutant embryos (Fig. 1E). All three ES cell clones transmitted the targeted allele through the germ line, and mice from the three lines displayed identical mutant phenotypes.

Disruption of Vezf1 results in vascular defects and lethality in homozygous and heterozygous embryos

The Vezf1 mutation was examined in the C57BL/6 background. Heterozygous *Vezf1*$^{+/-}$ mice were viable, fertile, and appeared phenotypically indistinguishable from their wild type littermates. In contrast, no viable *Vezf1*$^{-/-}$ offspring were obtained (Table 1). Embryonic death and intraembryonic hemorrhage of the Vezf1 KO phenotype became apparent at E9.5 (Table 1, Fig. 2A). Hemorrhaging, retarded, or resorbed *Vezf1*$^{-/-}$ embryos at sub-Mendelian ratios were found up to E16.5 (Table 1, Fig. 4A). Beginning at E12.5, about 20% of heterozygous embryos (10 out of 46; 22%) displayed localized edema and hemorrhaging in the back and neck (Table 1, Fig. 8A). At E13.5, these mutant *Vezf1*$^{+/-}$ embryos (7 out of 32; 22%) appeared

bloated, displaying massive edema, hemorrhaging, and signs of tissue necrosis in the back and neck (Table1, Fig. 8C). Hemorrhaging *Vezf1*$^{+/-}$ embryos were not detected at later embryonic stages and presumably died before E14.5. Consistent with this notion, heterozygous offspring (total 296) from backcrosses into the C57Bl/6 strain were recovered at a ratio of 41% *Vezf1*$^{+/-}$: 59% wild type.

In a mixed and outbred genetic background, a less severe and less penetrant phenotype was observed (Table 2), suggesting contribution of yet unknown strain-specific segregating modifier genes. Whereas no viable *Vezf1*$^{-/-}$ offspring were recovered at weaning age, stillborn P0 *Vezf1*$^{-/-}$ pups displaying intraembryonic hemorrhage were detected at a ratio of ~60% of the expected Mendelian frequency. *Vezf1*$^{-/-}$ embryos appeared phenotypically normal up to E11.5 of development. Between E12.5 and birth, Vezf1 KO embryos displayed varying degrees of intraembryonic bleeding and vascular malformations in the head and trunk region, or they were resorbed (data not shown). Vascular abnormalities were also observed in heterozygous mutant embryos, albeit at a low frequency (~10%).

In summary, loss of Vezf1 function resulted in an incompletely penetrant, haploinsufficient (autosomal) phenotype that was not caused by imprinting of the Vezf1 gene or by generation of a dominant-negative allele.

Vascular remodeling defects and hemorrhaging in early midgestation Vezf1$^{-/-}$ embryos

The developing vasculature in overtly hemorrhaging Vezf1 KO embryos and yolk sacs was examined in detail by whole-mount immunostaining for the pan-endothelial marker PECAM-1 (Baldwin et al., 1994) between E9.5 and E10.5. Wild type and *Vezf1*$^{+/-}$ littermates exhibited a complex, hierarchically organized vessel architecture throughout the entire embryo. *Vezf1*$^{-/-}$ mutant embryos had normally formed major vessels, like dorsal aorta and cardinal vein, but displayed prominent angiogenic remodeling defects in the vascular networks of the head, the aortic arch artery system, the heart, and the trunk. Thus, the vasculature in head, neck, and back in homozygous mutant Vezf1 embryos showed poor organization, was less branched, and appeared underdeveloped (compare E9.5 Vezf1 KO and wild type embryos in Figs. 2B and E). Furthermore, the first and second aortic arch arteries frequently had failed to develop in Vezf1 KO embryos (Figs. 2B and E). The remodeling defects were more pronounced at E10.5, with an increased disorganization of the trunk vessels and further deterioration of the arch arteries (not shown). Histological analysis of parasagittal sections through PECAM-1-stained *Vezf1*$^{-/-}$ embryos revealed distinct sites of internal bleeding, typically in the head, heart, and trunk, and confirmed the defects in the aortic arch artery system. In the representative Vezf1 KO embryo shown in Fig. 2C, the pericardial cavity was enlarged and filled with blood, and an unusual number of dilated, hemorrhaging vessels was detectable in the head. In addition, the agenesis of the second aortic arch artery and a rudimentary, lumen-less first aortic arch artery were apparent.

In contrast to the observed abnormalities in the embryo proper, no vascular defects were detected in the extraembryonic yolk sac, the initial site of endothelial and hematopoietic differentiation. Whole-mount PECAM-1 staining of E9.5 and E10.5 yolk sacs from mutant embryos showed a hierarchical vascular pattern that was indistinguishable from that of wild type controls (compare Figs. 3A and B). Furthermore, PECAM-1-stained sections of mutant yolk sacs displayed normally developed blood islands with an outer layer of endothelial cells surrounding lumens that are filled with primitive, nucleated erythrocytes, and regular vascular patterning without any signs of lesions or hemorrhaging (compare Figs. 3C and D).

Localized hemorrhaging in mutant Vezf1$^{-/-}$ embryos at late midgestation stages

A small fraction of homozygous mutant embryos survived to day 16 of gestation. These late midgestation KO embryos displayed localized hemorrhaging with incomplete penetrance (Table 1, Fig. 4A). Mutant E12.5 *Vezf1*$^{-/-}$ embryos did not display grossly abnormal vascular patterning as visualized by PECAM-1 antibody staining of parasagittal sections (Figs. 4E and F), consistent with mostly normal angiogenic remodeling. In addition, development of all organ systems, including heart, lung, and placenta, appeared normal in H&E-stained histological sections (Figs. 4C and D). However, localized hemorrhaging, typically in the head and in the neck region, was observed in these embryos, indicating the loss of vascular integrity (see below). The representative E12.5 *Vezf1*$^{-/-}$ embryo shown in Fig. 4C displays hemorrhaging in the subcapsular mesenchyme of the head and in the jugular region.

Normal vascular smooth muscle cell recruitment and megakaryocyte development in Vezf1 KO embryos

Defects in the differentiation and/or recruitment of VSMC or pericytes can result in destabilized, leaky blood vessels and lead to lethal hemorrhage, as has been shown in mice lacking Edg-1, LKLF, and PDGF-B (Kuo et al., 1997; Lindahl et al., 1997; Liu et al., 2000). To investigate a possible involvement of VSMC in the hemorrhaging observed in mutant E12.5 *Vezf1*$^{-/-}$ embryos, parasagittal sections of embryos shown in Fig. 4 were immunostained with anti-SM a-actin antibodies. In sections of *Vezf1*$^{-/-}$ and wild type control embryos, the dorsal aorta was completely surrounded by VSMCs (Figs. 4G and H). Likewise, cross sections through the dorsal aorta (Figs. 4I and J) and umbilical artery (not shown) of mutant embryos showed several layers of VSMC.

Likewise, defects in the differentiation of megakaryocytes can lead to defective platelet formation and control of coagulation, resulting ultimately in lethal hemorrhaging (Spyropoulos et al., 2000). To address whether megakaryocytopoiesis was affected in Vezf1 KO embryos, wild type and *Vezf1*$^{-/-}$ E12.5 fetal liver cells were cultured and assayed in vitro for their differentiation potential into megakaryocytes (Lecine et al., 1998). Normal megakaryocyte and proplatelet differentiation was apparent in day 5 in vitro cultures and Wright–Giemsa-stained cytospin preparations derived from homozygous mutant fetal liver cultures (Figs. 4K and L). Thus, defects in mural cell recruitment and megakaryocyte differentiation can be excluded as a cause for the vascular defects in E12.5 *Vezf1*$^{-/-}$ embryos.

Vascular endothelial integrity is compromised in hemorrhaging vessels

To understand the etiology of vascular leakage, we performed ultrastructural analysis on hemorrhaging vessels using transmission electron microscopy. Frontal sections through heads of E11.5 mutant embryos in regions of visible hemorrhaging revealed striking abnormalities (Fig. 5). Leaky capillaries and small blood vessels were easily found in the meningeal plexus. They displayed gaps between endothelial cells (Figs. 5A, C, and E) or incomplete cell–cell junctions. Frequently, extravasation of nucleated fetal erythrocytes could be detected at these gaps (Figs. 5A, B, and G). The endothelial cells often appeared discontinuous and fragmented (Figs. 5C and D) and had abnormal filopodia-like protrusions (Figs. 5A and B) and excessive fenestration (Fig. 5D). Under high magnification, an incomplete basal lamina could be discerned (Fig. 5G). The leaky vessels were localized immediately adjacent to the pia mater or at more distal sites in the meningeal plexus. In contrast, the small vessels embedded in the brain mesenchyme did not show signs of leakiness (Fig. 5H) and were indistinguishable from capillaries of wild type littermates (Fig. 5I).

We further examined the molecular basis for the endothelial cell defects. Using co-immunostaining and confocal imaging of sections from dorsal regions of hemorrhaging embryos shown in Fig. 5, we investigated the distribution of the tight junction protein ZO-1,

the intercellular adhesion protein VE-cadherin, the ECM protein Collagen IV, and PECAM-1 (Fig. 6). In the endothelial wall of mutant E11.5 embryos, fluorescent localization of both anti-ZO-1 and anti-VE-cadherin had a disrupted pattern that was significantly reduced when compared to that of wild type littermates (Figs. 6A–C). Similarly, reduced levels of Collagen IV deposition were detected in hemorrhaging embryos (Fig. 6D). In contrast, localization of PECAM-1 was comparable between wild type and mutant capillaries. A similar spotty, discontinuous ZO-1 pattern, and reduced and disjointed Collagen IV deposition, were found in the vessels and capillaries of E10.5 *Vezf1*$^{-/-}$ embryos that did not show hemorrhaging or overt vascular abnormalities (Figs. 7A and B). These findings indicate that loss of Vezf1 function leads to defects in endothelial cell junctions and extracellular matrix organization, and that these defects are present before overt vascular abnormalities and hemorrhaging become visible.

Vascular malformations and hemorrhaging in E13.5 embryos heterozygous for the targeted Vezf1 allele

Beginning at E12.5, hemorrhaging and edema, confined mostly to the jugular region, became apparent in about 20% of *Vezf1*$^{+/-}$ embryos (Table 1; compare Figs. 8A and B). By E13.5, embryos appeared bloated and displayed massive edema and bleeding in the back and neck region (compare Figs. 8C and D). H&E-stained parasagittal sections showed severe edema, with masses of loose connective tissue and mesenchymal cells separated by interstitial fluid, and subcutaneous bleeding in the back and neck region (Figs. 8E and I). Furthermore, a dramatic increase in vessel number was detected in close association with the jugular sac (Figs. 8E and I) when compared to wild type controls (Figs. 8F and J). PECAM-1 staining revealed that *Vezf1*$^{+/-}$ embryos displayed an overall normal looking vascular pattern and that hypervascularization appeared confined to the jugular region (Fig. 8, compare panels G, K, O to panels H, L, P). Vessels in the jugular region appeared enlarged, irregular shaped, and anastomosing, and they were occasionally filled with blood (Figs. 8K and M). Under high-power magnification, sites of vascular lesions were visible with erythrocytes leaking out into the surrounding mesenchymal tissue (Fig. 8N), indicating loss of vessel integrity. Quantitative morphometric analysis of PECAM-1-stained sections confirmed that the overall vessel number and the total vessel area were increased in the mid–back region of mutant heterozygous embryos by approximately 50% and 130%, respectively (Figs. 9A and B). Together, these results suggest that localized endothelial hyperproliferation in the jugular region leads to the formation of aberrant, dysfunctional vessels in heterozygous embryos.

Lymphatic hypervascularization in E13.5 Vezf1$^{+/-}$ mutant embryos

Hypervascularization in mutant *Vezf1*$^{+/-}$ embryos was observed specifically in the jugular region, which constitutes the first major site of lymphatic development (Sabin, 1909). Thus, lymphatic vessel formation in E13.5 wild type and *Vezf1*$^{+/-}$ embryos was analyzed by immunostaining for the lymphatic markers VEGFR-3 (Kaipainen et al., 1995), LYVE-1 (Banerji et al., 1999), and Prox1 (Wigle and Oliver, 1999). In wild type embryos, expression of VEGFR-3 (Figs. 10B and H) and LYVE-1 (Figs. 10D and J) was detected in the endothelium lining the jugular sac and in small capillaries of the neck mesenchyme. In *Vezf1*$^{+/-}$ embryos, in addition to these structures, the hyperplastic vessels in the jugular region stained positive for the two lymphatic markers (VEGFR-3, Fig. 10A and G; LYVE-1, Figs. 10C and I), but did not express SMa-actin (Figs. 10E and F) or desmin (not shown), indicating the absence of vessel-associated vascular smooth muscle cells and pericytes, respectively. Likewise, double immunofluorescence staining for PECAM-1 and Prox1 revealed that the majority of the aberrant vessels in the jugular region of heterozygous embryos display lymphatic characteristics (Figs. 10K and L), whereas in wild type controls only a subset of small capillaries appear to be lymphatics (Figs. 10M and N). In summary, our results indicate that the hyperplastic vessels in *Vezf1*$^{+/-}$ embryos are of lymphatic nature and that loss of a single

Vezf1 allele leads to lymphatic hypervascularization in the jugular region. Lymphatic defects in heterozygous embryos could not be detected at later embryonic stages (>E14.5) nor in juvenile or adult heterozygous Vezf1 offspring.

Gene expression analysis

Our results indicate that loss of Vezf1 function leads to defects in endothelial cell proliferation, angiogenic remodeling, and maintenance of vascular integrity. A number of factors have been implicated in these processes and shown to display similar or partially overlapping mutant phenotypes in gene inactivation studies (Carmeliet, 2000). To assess if loss of Vezf1 function could be correlated with changes in expression levels for any of these factors, semi-quantitative reverse transcriptase polymerase chain reaction (RT-PCR) analysis was performed on total RNA isolated from E10.5 *Vezf1*$^{-/-}$ embryos and wild type littermates. Because of the incompletely penetrant phenotype, E10.5 Vezf1 KO embryos were selected that displayed clear signs of hemorrhaging and vascular malformations. Expression of the following groups of genes was examined (Fig. 11): (1) VEGF-A, -C, and -D, and VEGFR-1, -2, and -3; (2) Angiopoietin-1 and -2, their cognate tyrosine kinase receptor Tie2, and the closely related orphan receptor Tie1 (Gale and Yancopoulos, 1999); (3) Notch1, Notch4, and its ligand Dll4 that have been implicated in vascular morphogenesis (Krebs et al., 2000); (4) EphrinB2 and its receptor EphB4 that demarcate embryonic arterial versus venous endothelium and are involved in vascular remodeling (Adams et al., 1999; Krebs et al., 2000; Wang et al., 1998); (5) LKLF, a Krüppel-like zinc finger transcription factor, Edg-1, the G-protein-coupled receptor for sphingosine-1-phosphate, and Endoglin, an accessory TGF-h-receptor, all of which show hemorrhaging KO phenotypes (Kuo et al., 1997; Li et al., 1999, 2000); (6) Prox-1 and podoplanin, two markers for lymphatic vessels (Wigle et al., 2002) (Breiteneder-Geleff et al., 1999); (7) Tbx-1, a T-box transcription factor required for development of the aortic arch artery system in a gene-dosage dependent manner (Lindsay et al., 2001); (8) VE-cadherin, an endothelial cell adhesion molecule and regulator of endothelial cell survival (Carmeliet et al., 1999); (9) Endothelin-1 (ET-1), a vaso-constrictive signaling peptide. ET-1 inactivation leads to malformations in the aortic arch system (Kurihara et al., 1994), and the human ET-1 promoter is transactivated by ZNF161/DB1 in vitro (Aitsebaomo et al., 2001). As expected, Vezf1 transcripts were absent in E10.5 *Vezf1*$^{-/-}$ embryos and present in wild type littermates. In contrast, no differences in the expression of any of the candidate genes examined were found between mutant and wild type embryos (Fig. 11). In addition, the distribution of transcripts for Flk-1, Flt-1, EphrinB2, Tie2, and ET-1 was analyzed by RNA in situ hybridization on E11.5 embryos. No differences in the amount or spatial distribution of these transcripts between *Vezf1*$^{-/-}$ and wild type embryos were detected (data not shown). Thus, Vezf1 function is not required for the expression of these candidate genes known to regulate mammalian vasculogenesis and angiogenesis.

Discussion

We report here that Vezf1 is essential for normal development of the vascular system. Inactivation of Vezf1 leads to embryonic lethality, and mutant embryos display specific defects during angiogenic remodeling, vascular homeostasis, and lymphatic development. Analysis of the homozygous mutant phenotype revealed that, while its function is dispensable for the early stages of vascular development, namely angioblast differentiation and the formation of the primary vascular plexus, Vezf1 is required for proper angiogenic remodeling and the maintenance of vascular integrity. Homozygous mutant embryos can be subdivided into two classes. Class 1 embryos display an early phenotype that is characterized by defective angiogenic remodeling, particularly in the developing vasculature of the aortic arch system, the head and neck, and in the intersomitic vessels, and by the loss of vascular integrity leading to hemorrhaging. In contrast, class 2 embryos display apparently normal vascular patterning

but are subject to midgestation hemorrhaging. The manifestation of vascular leakage in these later stage KO embryos without concomitant vascular dysmorphogenesis suggests that hemorrhaging in class 1 embryos is independent of the angiogenic remodeling defects. This notion is further supported by the fact that similar remodeling defects were reported for the inactivation of Angiopoietin1, Tie2, VEGFR-3, ephrinB2, EphB4, EphB2/B3, and Notch1/Notch4, and that these mutants did not display any vascular leakage (Adams et al., 1999; Detmar et al., 1998; Gerety et al., 1999; Krebs et al., 2000; Sato et al., 1995; Sun et al., 1996; Wang et al., 1998). Interestingly, in those studies, abnormal vascular remodeling was also observed in the extraembryonic yolk sac, whereas the yolk sac vasculature appeared normal in Vezf1 KO embryos. A plausible explanation is that Vezf1 acts in a combinatorial fashion with other co-factors and therefore differentially controls diverse developmental processes. We hypothesize that Vezf1 function is dispensable for the yolk sac vasculature or that redundant regular pathways can compensate for loss of Vezf1.

Our studies strongly suggest that at the cellular level the primary defect has its origin in the vascular endothelial cells themselves. First, Vezf1 is expressed in endothelial cells during embryogenesis (Xiong et al., 1999). Second and most importantly, ultrastructural and immunohistochemistry studies directly show loss of vascular wall integrity in hemorrhaging vessels due to the apparent lack of proper formation of inter-endothelial cell junctions and the interaction of endothelial cells with or the formation of the basal membrane in these cells. Notably, defects in endothelial cell junctions and basal membrane were detected even before the onset of the mutant phenotype. Thus, these endothelial cell defects likely predispose vessels and capillaries to loss of their integrity, possibly in a stochastic manner. Third, two alternative causes were addressed in this study, namely defects in VSMC differentiation and/or recruitment (Kuo et al., 1997; Liu et al., 2000) and defective megakaryocyte differentiation (Spyropoulos et al., 2000). However, both processes were found to be normal in homozygous mutant embryos. Fourth, our preliminary studies indicate that embryonic lethality in Vezf1 KO embryos can be rescued by endothelial overexpression of Vezf1 via a Tie2–Vezf1 transgene (Z. Zou, F. Kuhnert, and H. Stuhlmann, unpublished). It is possible that additional cell-non-autonomous effects by mesenchymal cells, vascular smooth muscle cells, or pericytes contribute to the vascular phenotype as well. Generation of Vezf1 conditional null alleles targeted to the endothelial and smooth muscle cell lineages will provide answers to this question.

The specific defects in cell–cell adhesion and tight junction formation provide first insights into potential molecular pathways in which Vezf1 participates. In this context, it is of interest that our candidate gene approach has not identified thus far in vivo downstream target genes. In this study, the expression of a large canon of genes known to regulate endothelial cell proliferation, angiogenic remodeling, and the maintenance of vascular integrity was examined. Loss of Vezf1 function could not be correlated with changes in the expression levels for any of these genes. In a recent study, in vitro binding and transactivation of the human ET-1 promoter by ZNF161/DB1, the human ortholog of Vezf1, was demonstrated (Aitsebaomo et al., 2001). Interestingly, mice deficient for ET-1 display defects in the aortic arch artery system (Kurihara et al., 1994, 1995). However, no effects of Vezf1 inactivation on ET-1 transcript levels and its spatial distribution could be detected. Furthermore, during the preparation of the manuscript, a report by Miyashita et al. identified the microtubule-destabilizing protein stathmin/OP18 as a potential in vitro target of VEZF1 (Miyashita et al., 2004). A microarray expression profiling approach using Vezf1 KO and wild type endothelial cells should be instrumental in identifying Vezf1 target genes and thus provide further insights into the molecular mechanisms that underlie Vezf1 function.

Our results indicate that Vezf1 acts in a closely regulated, dose-dependent manner during vascular development. Approximately 20% of heterozygous embryos displayed lymphatic

hypervascularization in the jugular region, associated with edema and hemorrhaging. This incompletely penetrant, haploinsufficient (autosomal) phenotype is caused neither by imprinting of the residual wild type allele, nor by the generation of a dominant-negative VEZF1 mutant peptide. Several other examples of haploinsufficiency in genes crucial for vascular development have been reported; these include VEGF-A, TGF-h, the T-box transcription factor Tbx-1, and the Notch ligand Delta4 (Carmeliet et al., 1996b; Dickson et al., 1995; Duarte et al., 2004; Ferrara et al., 1996; Krebs et al., 2004; Lindsay et al., 2001). However, Vezf1 appears to be the only vascular haploinsufficiency gene that affects lymphatic development.

Our results indicate that Vezf1 is involved in the regulation of early events of lymphangiogenesis, as lymphatic hypervascularization is specifically observed in the jugular region, the first site of lymphatic sprouting from the venous system. The increased vascularity suggests lymphatic endothelial hyperproliferation or increased lymphatic endothelial differentiation as a plausible mechanism for the observed vascular hyperplasia and identifies Vezf1 as a negative regulator of lymphatic development. Support for this notion comes from recent studies in which knock-down of the human ortholog DB1 in primary endothelial cells leads to an increase in lymphatic phenotype and gene expression (I. Adini and L. Benjamin, personal communication). A low incidence of vascular defects in the jugular region of homozygous mutant embryos, albeit less pronounced than in affected heterozygotes (Fig. 4C), could be detected (4 out of 17 *Vezf1*$^{-/-}$ embryos obtained between E12.5 and E14.5). We surmise that the early lethality in *Vezf1*$^{-/-}$ embryos in combination with the apparent genetic background susceptibility of the lymphatic phenotype precluded a more robust detection (both in frequency and severity) in homozygous mutant embryos.

The lymphatic nature of the hyperplastic vessels appears to conflict with the fact that many of these contain red blood cells. However, it has been reported that lymphatic capillaries may contain stagnant blood, which is removed into the venous circulation once the lymphatic system becomes functional (Clark, 1912; Lewis, 1905; Miller, 1913). Alternatively, separation of the emerging lymphatic vessels from the blood vasculature may be defective in the mutant mice, similar to the phenotype recently reported for the inactivation of the hematopoietic signaling proteins SLP-76 and Syk (Abtahian et al., 2003). Of interest, severe edema and hemorrhaging were not detected at later embryonic stages, in other regions of embryonic lymphangiogenesis, or in heterozygous juvenile or adult offspring. We therefore hypothesize that a specific window, both temporal and spatial, exists during which lymphangiogenesis is susceptible to loss of Vezf1.

Lymphatic development is initiated by budding and sprouting of Prox1 and LYVE-1-positive cells from the anterior cardinal vein at around E10 (Oliver and Harvey, 2002). The nascent lymphatic endothelial cells migrate dorsoanteriorly to form the jugular lymph sacs. Prox1 activity is required for maintaining sprouting of lymphatic endothelial cells, and loss of Prox1 function results in the arrest of lymphatic development (Wigle and Oliver, 1999; Wigle et al., 2002). Careful etiological analysis will be necessary to further elucidate the mechanism underlying the lymphatic phenotype in *Vezf1*$^{+/-}$ embryos. For example, it will be important to examine if overexpression of Vezf1 in blood endothelial cells antagonizes Prox1 function, and if forced Vezf1 expression in lymphatic endothelial cells has anti-proliferative or anti-differentiation effects.

The haploinsufficient lymphatic phenotype observed in E13.5 *Vezf1*$^{+/-}$ embryos is reminiscent of a human malformation syndrome, cystic hygroma. Cystic hygromas are congenital malformations of the lymphatic system that occur at sites of lymphatic-venous connection, most commonly in the posterior neck (Gallagher et al., 1999). Typically, cystic hygromas develop late in the first trimester, either as a consequence of failure of the lymphatic vessels to connect to the venous system, leading to the accumulation of fluid in dilated lymphatics and

to progressive lymphedema, or due to abnormal budding of lymphatic endothelium (Edwards and Graham, 1990). Although cystic hygromas are frequently associated with other malformation syndromes characterized by chromosomal abnormalities, such as Turner syndrome or Trisomy 21, fetal nuchal cystic hygromas with normal karyotypes have been reported (Marchese et al., 1985). It will be important to examine if haploinsufficiency of the human ortholog ZNF161/DB1 is associated with this human syndrome. Moreover, it will be interesting to determine if loss of ZNF161/DB1 function can be correlated with other known hyperplastic conditions thought to arise by excessive proliferation of lymphatic endothelial cells, such as lymphangioma, lymphangiosarcoma, and Kaposi's sarcoma (Witte et al., 1997).

In summary, our results identify Vezf1 as a gene whose function is crucial for the normal development of blood and lymphatic vasculature in mice in a dosage-dependent manner. At the cellular level, Vezf1 acts cell-autonomously in endothelial cells and affects integrity and proliferation of the developing vessels. Vezf1 might participate in yet unknown pathways that affect vascular differentiation and endothelial proliferation. To elucidate these molecular pathways, it will be important to identify genes that function in the same transcriptional regulatory circuits as VEZF1.

Acknowledgments

We would like to acknowledge Dr. Nissi Varki (UC San Diego School of Medicine) on the pathology of the mutant Vezf1 mice, Dr. Kevin Kelly (Mount Sinai School of Medicine Transgenic Core) for blastocyst injections, and Dr. Malcolm Wood (Scripps Core Microscopy Facility) for electron microscopy. We thank Drs. Seji Tadokoro and Sanford Shattil for advice with megakaryocyte cultures and Wendy LeVine for expert technical assistance with mouse husbandry, histology, and immunohistochemistry. We are thankful to Drs. K. Andrikopoulous and F. Ramirez (Mount Sinai School of Medicine, New York) for the mouse genomic 129/SV lambda library; and Drs. H. Kubo and K. Aritalo, D. Jackson, and G. Oliver for providing us with antibodies to mouse VEGFR-3, LYVE-1, and Prox1, respectively. We thank Dr. Ullrich Müller and members of the Stuhlmann lab for critical comments on the manuscript and Kathy Kling for help with preparing the manuscript. This work was supported by NIH grants R29 HD31534 and R01 HL65738, and Grant-in-Aid #99505N from the American Heart Association-National Center, to H.S. J.-W.X. was supported in part by a NIH training grant (T32 DK07757).

References

Abtahian F, Guerriero A, Sebzda E, Lu MM, Zhou R, Mocsai A, Myers EE, Huang B, Jackson DG, Ferrari VA, Tybulewicz V, Lowell CA, Lepore JJ, Koretzky GA, Kahn ML. Regulation of blood and lymphatic vascular separation by signaling proteins SLP-76 and Syk. Science 2003;299:247–251. [PubMed: 12522250]

Adams RH, Wilkinson GA, Weiss C, Diella F, Gale NW, Deutsch U, Risau W, Klein R. Roles of ephrinB ligands and EphB receptors in cardiovascular development: demarcation of arterial/venous domains, vascular morphogenesis, and sprouting angiogenesis. Genes Dev 1999;13:295–306. [PubMed: 9990854]

Aitsebaomo J, Kingsley-Kallesen ML, Wu Y, Quertermous T, Patterson C. Vezf1/DB1 is an endothelial cell-specific transcription factor that regulates expression of the endothelin-1 promoter. J. Biol. Chem 2001;14:14.

Baldwin HS, Shen HM, Yan HC, DeLisser HM, Chung A, Mickanin C, Trask T, Kirschbaum NE, Newman PJ, Albelda SM, et al. Platelet endothelial cell adhesion molecule-1 (PECAM-1/CD31): alternatively spliced, functionally distinct isoforms expressed during mammalian cardiovascular development. Development 1994;120:2539–2553. [PubMed: 7956830]

Banerji S, Ni J, Wang SX, Clasper S, Su J, Tammi R, Jones M, Jackson DG. LYVE-1, a new homologue of the CD44 glycoprotein, is a lymph-specific receptor for hyaluronan. J. Cell Biol 1999;144:789–801. [PubMed: 10037799]

Breiteneder-Geleff S, Soleiman A, Kowalski H, Horvat R, Amann G, Kriehuber E, Diem K, Weninger W, Tschachler E, Alitalo K, Kerjaschki D. Angiosarcomas express mixed endothelial phenotypes of blood and lymphatic capillaries: podoplanin as a specific marker for lymphatic endothelium. Am. J. Pathol 1999;154:385–394. [PubMed: 10027397]

Carmeliet P. Mechanisms of angiogenesis and arteriogenesis. Nat. Med 2000;6:389–395. [PubMed: 10742145]

Carmeliet P, Ferreira V, Breier G, Pollefeyt S, Kieckens L, Gertsenstein M, Fahrig M, Vandenhoeck A, Harpal K, Eberhardt C, Declercq D, Pawling J, Moons L, Collen D, Risau W, Nagy A. Abnormal blood vessel development and lethality in embryos lacking a single VEGF allele. Nature 1996a; 380:435–439. [PubMed: 8602241]

Carmeliet P, Mackman N, Moons L, Luther T, Gressens P, Van Vlaenderen I, Demunck H, Kasper M, Breier G, Evrard P, Muller M, Risau W, Edgington T, Collen D. Role of tissue factor in embryonic blood vessel development. Nature 1996b;383:73–75. [PubMed: 8779717]

Carmeliet P, Lampugnani MG, Moons L, Breviario F, Compernolle V, Bono F, Balconi G, Spagnuolo R, Oostuyse B, Dewerchin M, Zanetti A, Angellilo A, Mattot V, Nuyens D, Lutgens E, Clotman F, de Ruiter MC, Gittenberger-de Groot A, Poelmann R, Lupu F, Herbert JM, Collen D, Dejana E. Targeted deficiency or cytosolic truncation of the VE-cadherin gene in mice impairs VEGF-mediated endothelial survival and angiogenesis. Cell 1999;98:147–157. [PubMed: 10428027]

Clark EL. General observations on early superficial lymphatics in living chick embryos. Anat. Rec 1912;6:247–251.

Detmar M, Brown LF, Schon MP, Elicker BM, Velasco P, Richard L, Fukumura D, Monsky W, Claffey KP, Jain RK. Increased microvascular density and enhanced leukocyte rolling and adhesion in the skin of VEGF transgenic mice. J. Invest. Dermatol 1998;111:1–6. [PubMed: 9665379]

Dickson MC, Martin JS, Cousins FM, Kulkarni AB, Karlsson S, Akhurst RJ. Defective hematopoiesis and vasculogenesis in transforming growth factor-b1 knock out mice. Development 1995;121:1845–1854. [PubMed: 7600998]

Duarte A, Hirashima M, Benedito R, Trindade A, Diniz P, Bekman E, Costa L, Henrique D, Rossant J. Dosage-sensitive requirement for mouse Dll4 in artery development. Genes Dev 2004;18:2474–2478. [PubMed: 15466159]

Edwards MJ, Graham JM Jr. Posterior nuchal cystic hygroma. Clin. Perinatol 1990;17:611–640. [PubMed: 2225690]

Ferrara N, Carver-Moore K, Chen H, Dowd M, Lu L, O'Shea KS, Powell-Braxton L, Hillan KJ, Moore MW. Heterozygous embryonic lethality induced by targeted inactivation of the VEGF gene. Nature 1996;380:439–442. [PubMed: 8602242]

Gale NW, Yancopoulos GD. Growth factors acting via endothelial cell-specific receptor tyrosine kinases: VEGFs, angiopoietins, and ephrins in vascular development. Genes Dev 1999;13:1055–1066. [PubMed: 10323857]

Gale NW, Thurston G, Hackett SF, Renard R, Wang Q, McClain J, Martin C, Witte C, Witte MH, Jackson D, Suri C, Campochiaro PA, Wiegand SJ, Yancopoulos GD. Angiopoietin-2 is required for postnatal angiogenesis and lymphatic patterning, and only the latter role is rescued by angiopoietin-1. Dev. Cell 2002;3:411–423. [PubMed: 12361603]

Gallagher PG, Mahoney MJ, Gosche JR. Cystic hygroma in the fetus and newborn. Semin. Perinatol 1999;23:341–356. [PubMed: 10475547]

Gerety SS, Wang HU, Chen ZF, Anderson DJ. Symmetrical mutant phenotypes of the receptor EphB4 and its specific transmembrane ligand ephrin-B2 in cardiovascular development. Mol. Cell 1999;4:403–414. [PubMed: 10518221]

Hong YK, Harvey N, Noh YH, Schacht V, Hirakawa S, Detmar M, Oliver G. Prox1 is a master control gene in the program specifying lymphatic endothelial cell fate. Dev. Dyn 2002;225:351–357. [PubMed: 12412020]

Iyer NV, Kotch LE, Agani F, Leung SW, Laughner E, Wenger RH, Gassmann M, Gearhart JD, Lawler AM, Yu AY, Semenza GL. Cellular and developmental control of O2 homeostasis by hypoxia-inducible factor 1a. Genes Dev 1998;12:149–162. [PubMed: 9436976]

Kaipainen A, Korhonen J, Mustonen T, van Hinsbergh VW, Fang GH, Dumont D, Breitman M, Alitalo K. Expression of the fms-like tyrosine kinase 4 gene becomes restricted to lymphatic endothelium during development. Proc. Natl. Acad. Sci. U. S. A 1995;92:3566–3570. [PubMed: 7724599]

Karkkainen MJ, Ferrell RE, Lawrence EC, Kimak MA, Levinson KL, McTigue MA, Alitalo K, Finegold DN. Missense mutations interfere with VEGFR-3 signalling in primary lymphoedema. Nat. Genet 2000;25:153–159. [PubMed: 10835628]

Karkkainen MJ, Haiko P, Sainio K, Partanen J, Taipale J, Petrova TV, Jeltsch M, Jackson DG, Talikka M, Rauvala H, Betsholtz C, Alitalo K. Vascular endothelial growth factor C is required for sprouting of the first lymphatic vessels from embryonic veins. Nat. Immunol 2004;5:74–80. [PubMed: 14634646]

Krebs LT, Xue Y, Norton CR, Shutter JR, Maguire M, Sundberg JP, Gallahan D, Closson V, Kitajewski J, Callahan R, Smith GH, Stark KL, Gridley T. Notch signaling is essential for vascular morphogenesis in mice. Genes Dev 2000;14:1343–1352. [PubMed: 10837027]

Krebs LT, Shutter JR, Tanigaki K, Honjo T, Stark KL, Gridley T. Haploinsufficient lethality and formation of arteriovenous malformations in Notch pathway mutants. Genes Dev 2004;18:2469–2473. [PubMed: 15466160]

Kubo H, Fujiwara T, Jussila L, Hashi H, Ogawa M, Shimizu K, Awane M, Sakai Y, Takabayashi A, Alitalo K, Yamaoka Y, Nishikawa SI. Involvement of vascular endothelial growth factor receptor-3 in maintenance of integrity of endothelial cell lining during tumor angiogenesis. Blood 2000;96:546–553. [PubMed: 10887117]

Kuo CT, Veselits ML, Barton KP, Lu MM, Clendenin C, Leiden JM. The LKLF transcription factor is required for normal tunica media formation and blood vessel stabilization during murine embryogenesis. Genes Dev 1997;11:2996–3006. [PubMed: 9367982]

Kurihara Y, Kurihara H, Suzuki H, Kodama T, Maemura K, Nagai R, Oda H, Kuwaki T, Cao WH, Kamada N, et al. Elevated blood pressure and craniofacial abnormalities in mice deficient in endothelin-1. Nature 1994;368:703–710. [PubMed: 8152482]

Kurihara Y, Kurihara H, Oda H, Maemura K, Nagai R, Ishikawa T, Yazaki Y. Aortic arch malformations and ventricular septal defect in mice deficient in endothelin-1. J. Clin. Invest 1995;96:293–300. [PubMed: 7615798]

Leahy A, Xiong J-W, Kuhnert F, Stuhlmann H. Use of developmental marker genes to define temporal and spatial patterns of differentiation during embryoid body formation. J. Exp. Zool 1999;284:67–81. [PubMed: 10368935]

Lecine P, Blank V, Shivdasani R. Characterization of the hematopoietic transcription factor NF-E2 in primary murine megakaryocytes. J. Biol. Chem 1998;273:7572–7578. [PubMed: 9516460]

Lemons D, Sun X, Zou Z, Campagnolo L, Xiong J-W, Kuhnert F, English M, Licht J, Stuhlmann H. VEZF1 is an endothelial transcriptional transactivator that dispays sequence-specific DNA binding to the IL-3, flk-1 and flt-1 promoter. 2005Under revision

Lewis F. The development of the lymphatic system in rabbits. Am. J. Anat 1905;5:95–121.

Li DY, Sorensen LK, Brooke BS, Urness LD, Davis EC, Taylor DG, Boak BB, Wendel DP. Defective angiogenesis in mice lacking Endoglin. Science 1999;284:1534–1537. [PubMed: 10348742]

Lindahl P, Johansson BR, Leveen P, Betsholtz C. Pericyte loss and microaneurysm formation in PDGF-B-deficient mice. Science 1997;277:242–245. [PubMed: 9211853]

Lindsay EA, Vitelli F, Su H, Morishima M, Huynh T, Pramparo T, Jurecic V, Ogunrinu G, Sutherland HF, Scambler PJ, Bradley A, Baldini A. Tbx1 haploinsufficieny in the DiGeorge syndrome region causes aortic arch defects in mice. Nature 2001;410:97–101. [PubMed: 11242049]

Liu Y, Wada R, Yamashita T, Mi Y, Deng CX, Hobson JP, Rosenfeldt HM, Nava VE, Chae SS, Lee MJ, Liu CH, Hla T, Spiegel S, Proia RL. Edg-1, the G protein-coupled receptor for sphingosine-1-phosphate, is essential for vascular maturation. J. Clin. Invest 2000;106:951–961. [PubMed: 11032855]

Makinen T, Jussila L, Veikkola T, Karpanen T, Kettunen MI, Pulkkanen KJ, Kauppinen R, Jackson DG, Kubo H, Nishikawa S, Yla-Herttuala S, Alitalo K. Inhibition of lymphangiogenesis with resulting lymphedema in transgenic mice expressing soluble VEGF receptor-3. Nat. Med 2001;7:199–205. [PubMed: 11175851]

Marchese C, Savin E, Dragone E, Carozzi F, De Marchi M, Campogrande M, Dolfin GC, Pagliano G, Viora E, Carbonara A. Cystic hygroma: prenatal diagnosis and genetic counselling. Prenatal Diagn 1985;5:221–227.

Miller AM. Histogenesis and morphogenesis of the thoracic duct in the chick; development of blood cells and their passage to the blood stream via the thoracic duct. Am. J. Anat 1913;15:131–198.

Miyashita H, Kanemura M, Yamazaki T, Abe M, Sato Y. Vascular endothelial zinc finger 1 is involved in the regulation of angiogenesis: possible contribution of stathmin/OP18 as a downstream target gene. Arterioscler., Thromb., Vasc. Biol 2004;24:878–884. [PubMed: 15031128]

Mortensen RM, Conner DA, Chao S, Geisterfer-Lowrance AA, Seidman JG. Production of homozygous mutant ES cells with a single targeting construct. Mol. Cell. Biol 1992;12:2391–2395. [PubMed: 1569957]

Nagy, A.; Rossant, J. Production of completely ES cell-derived fetuses. In: Joyner, AL., editor. Gene Targeting: A Practical Approach. Oxford Univ. Press; New York: 1993. p. 147-179.

Oettgen P. Transcriptional regulation of vascular development. Circ. Res 2001;89:380–388. [PubMed: 11532898]

Oliver G, Harvey N. A stepwise model of the development of lymphatic vasculature. Ann. N. Y. Acad. Sci 2002;979:159–165. [PubMed: 12543725]Discussion 188–196

Petrova TV, Makinen T, Makela TP, Saarela J, Virtanen I, Ferrell RE, Finegold DN, Kerjaschki D, Yla-Herttuala S, Alitalo K. Lymphatic endothelial reprogramming of vascular endothelial cells by the Prox-1 homeobox transcription factor. EMBO J 2002;21:4593–4599. [PubMed: 12198161]

Pozzi A, Moberg PE, Miles LA, Wagner S, Soloway P, Gardner HA. Elevated matrix metalloprotease and angiostatin levels in integrin alpha 1 knockout mice cause reduced tumor vascularization. Proc. Natl. Acad. Sci. U. S. A 2000;97:2202–2207. [PubMed: 10681423]

Prevo R, Banerji S, Ferguson DJ, Clasper S, Jackson DG. Mouse LYVE-1 is an endocytic receptor for hyaluronan in lymphatic endothelium. J. Biol. Chem 2001;276:19420–19430. [PubMed: 11278811]

Risau W. Mechanisms of angiogenesis. Nature 1997;386:671–674. [PubMed: 9109485]

Ryan HE, Lo J, Johnson RS. HIF-1 alpha is required for solid tumor formation and embryonic vascularization. EMBO J 1998;17:3005–3015. [PubMed: 9606183]

Sabin FR. The lymphatic system in human embryos, with a consideration of the morphology of the system as a whole. Am. J. Anat 1909;9:43–91.

Sato TM, Tozawa Y, Deutsch U, Wolburg-Buchholz K, Fujiwara Y, Gendron-Maguire M, Gridley T, Wolburg H, Risau W, Qin Y. Distinct roles of the receptor tyrosine kinases Tie-1 and Tie-2 in blood vessel formation. Nature 1995;376:70–74. [PubMed: 7596437]

Spyropoulos DD, Pharr PN, Lavenburg KR, Jackers P, Papas TS, Ogawa M, Watson DK. Hemorrhage, impaired hematopoiesis, and lethality in mouse embryos carrying a targeted disruption of the Fli1 transcription factor. Mol. Cell. Biol 2000;20:5643–5652. [PubMed: 10891501]

Sun L, Liu A, Georgopoulos K. Zinc finger-mediated protein interactions modulate Ikaros activity, a molecular control of lymphocyte development. EMBO J 1996;15:5358–5369. [PubMed: 8895580]

Veikkola T, Jussila L, Makinen T, Karpanen T, Jeltsch M, Petrova TV, Kubo H, Thurston G, McDonald DM, Achen MG, Stacker SA, Alitalo K. Signalling via vascular endothelial growth factor receptor-3 is sufficient for lymphangiogenesis in transgenic mice. EMBO J 2001;20:1223–1231. [PubMed: 11250889]

Wang W, Lufkin T. The murine Otp homeobox gene plays an essential role in the specification of neuronal cell lineages in the developing hypothalamus. Dev. Biol 2000;227:432–449. [PubMed: 11071765]

Wang HU, Chen Z-F, Anderson DJ. Molecular distinction and angiogenic interaction between embryonic arteries and veins revealed by ephrin-B2 and its receptor Eph-B4. Cell 1998;93:741–753. [PubMed: 9630219]

Wigle JT, Oliver G. Prox1 function is required for the development of the murine lymphatic system. Cell 1999;98:769–778. [PubMed: 10499794]

Wigle JT, Chowdhury K, Gruss P, Oliver G. Prox1 function is crucial for mouse lens-fibre elongation. Nat. Genet 1999;21:318–322. [PubMed: 10080188]

Wigle JT, Harvey N, Detmar M, Lagutina I, Grosveld G, Gunn MD, Jackson DG, Oliver G. An essential role for Prox1 in the induction of the lymphatic endothelial cell phenotype. EMBO J 2002;21:1505–1513. [PubMed: 11927535]

Witte MH, Way DL, Witte CL, Bernas M. Lymphangiogenesis: mechanisms, significance and clinical implications. EXS 1997;79:65–112. [PubMed: 9002221]

Xiong J-W, Leahy A, Lee H-H, Stuhlmann H. Vezf1: a Zn finger transcription factor restricted to endothelial cells and their precursors. Dev. Biol 1999;206:123–141. [PubMed: 9986727]

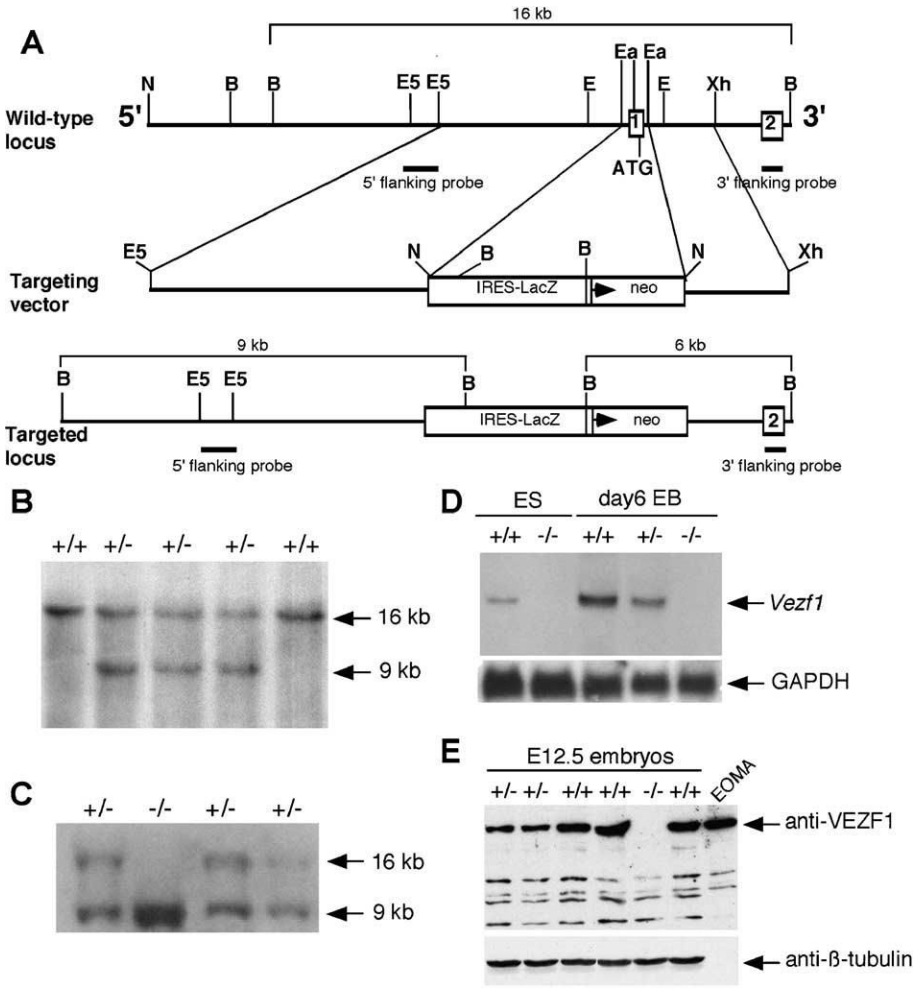

Fig. 1.

Targeted inactivation of the Vezf1 gene. (A) Targeting strategy. Exons are represented as numbered boxes. The first exon, 91 bp of upstream genomic DNA, and the proximal part of the first intron were replaced with an IRES-lacZ-neo expression cassette by homologous recombination in R1 ES cells. Regions of homology between the endogenous locus (top) and the targeting vector (middle) are indicated by lines. The structure of the targeted allele is shown on the bottom. Locations of probes for Southern analysis corresponding to 5′ and 3′ flanking regions are indicated by bars. B, BamHI; E, EagI; E5, EcoRV; N, NotI; X, XhoI. (B) Southern blot analysis of three correctly targeted ES cell clones. 10-Ag genomic DNA was digested with BamHI and hybridized with the 5′ flanking probe shown in (A). Sizes of hybridizing fragments are indicated. Genotypes of ES cell clones are indicated at the top of each lane. Three independent targeted *Vezf1*$^{+/-}$ ES cell clones (#2, 74, 86) were identified. (C) Southern blot analysis of DNA isolated from individual ES cell clones subjected G418 hyperselection protocol. Experimental procedures are identical to those in B. One *Vezf1*$^{-/-}$ clone (lane 2) was recovered. (D) Northern blot analysis of total RNA from ES cells and day 6 embryoid bodies using a Vezf1 cDNA fragment (nucleotides 3–776) as a probe. The filter was reprobed with a GAPDH-specific probe to control for loading. Genotypes are indicated at the top of each lane. No Vezf1-specific transcript was detected in *Vezf1*$^{-/-}$ ES cells and embryoid bodies. (E) Western blot analysis of total cell extracts from E12.5 embryos (genotypes are indicated) using VEZF1-specific antibodies. Nuclear extract from endothelioma cells (EOMA) was loaded as

a control. The filter was stripped and reprobed with an anti-h-tubulin antibody to control for equal loading.

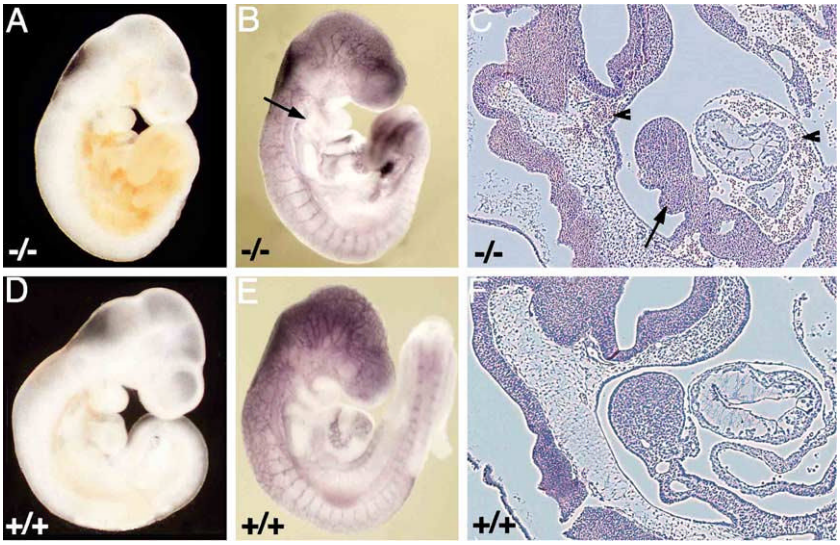

Fig. 2.

Vascular defects in E9.5 *Vezf1*$^{-/-}$ embryos. (A and D) Photomicrographs of E9.5 Vezf1 KO (-/-) and wild type (+/+) embryos. *Vezf1*$^{-/-}$ embryos displayed hemorrhaging in the head, the trunk, and the pericardial cavity. (B and E) Whole mount immunohistochemistry for PECAM-1. The vasculature in head, neck, and dorsal part of intersomitic vessels of *Vezf1*$^{-/-}$ embryos (B) appeared disorganized and less developed than in wild type controls (E). The arrow indicates absence of the second aortic arch artery in the *Vezf1*$^{-/-}$ embryo. (C and F) Histological sections of same E9.5 embryos. *Vezf1*$^{-/-}$ embryo (C) displayed hemorrhaging in the head and the pericardial cavity (arrowheads). Note also the absence of the second aortic arch artery (arrow). (F) Wild type control.

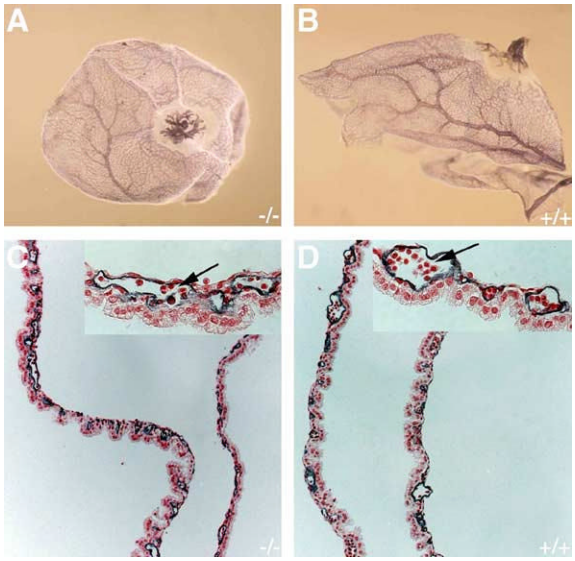

Fig. 3.

Normal vascular development in *Vezf1*$^{-/-}$ yolk sacs. (A and B) Photomicrographs of whole-mount PECAM-1-stained E9.5 yolk sacs. *Vezf1*$^{-/-}$ yolk sacs (A) displayed a regular hierarchical vascular pattern that is indistinguishable from that of wild type controls (B). (C and D) Sections of the same PECAM-1-stained yolk sacs were counterstained with Nuclear Fast Red. Inserts, details of yolk sacs at high magnification. Blood islands are lined by PECAM-1-postive endothelial cells and filled with primitive, nucleated erythrocytes (arrows). *Vezf1*$^{-/-}$ yolk sacs (C) did not show any signs of vascular disorganization or lesion. (D) Wild type control.

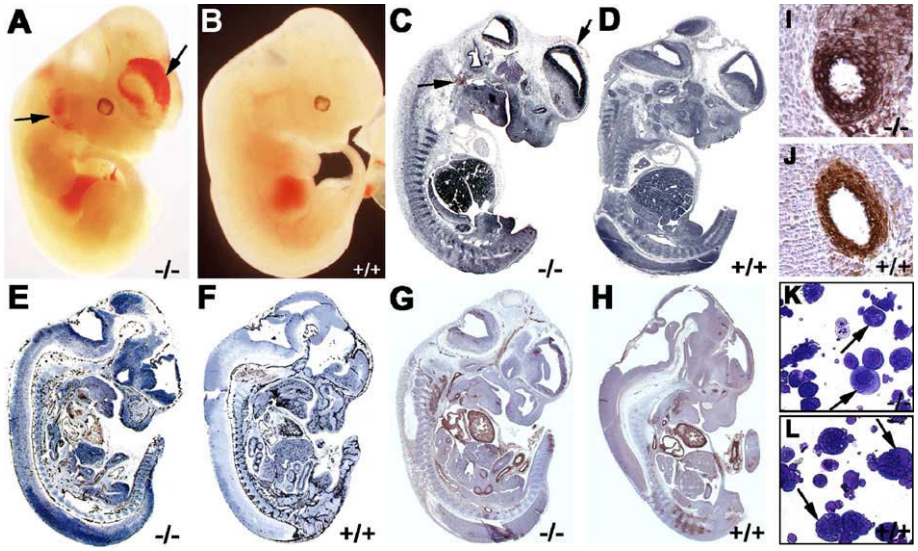

Fig. 4.

Hemorrhaging in E12.5 *Vezf1*$^{-/-}$ embryos. (A and B) Whole-mount images of E12.5 *Vezf1*$^{-/-}$ (A) and wild type (B) embryos. The E12.5 KO embryo displayed hemorrhaging in the jugular region and subcapsular head mesenchyme (arrows). Parasagittal sections shown in C, E, G are derived from the Vezf1 KO embryo depicted in A, and sections shown in D, F, H are from the wild type embryo depicted in B. (C and D) Histological analysis of H&E-stained E12.5 *Vezf1*$^{-/-}$ (C) and wild type (D) embryo. Arrows in C indicate sites of bleeding in the jugular region and the subcapsular head mesenchyme. (E and F) Immunohistochemical PECAM-1 staining revealed overall normal vascular patterning in *Vezf1*$^{-/-}$ (E) and wild type (F) embryos. (G and H) Immunohistochemical SMa-actin staining demonstrated normal VSMC differentiation and recruitment in Vezf1 KO (G) and wild type (H) embryos. (I and J) In transverse sections of anti-SMa-actin-stained embryos, the dorsal aorta is surrounded by several layers of VSMCs in Vezf1 KO (I) and wild type embryos (J). (K and L) Wright–Giemsa staining of day 5 in vitro cultures of E12.5 fetal liver cells shows normal megakaryopoiesis in *Vezf1*$^{-/-}$ embryos (K) as compared to a wild type control embryo (L). Arrows indicate examples of megakaryocytes.

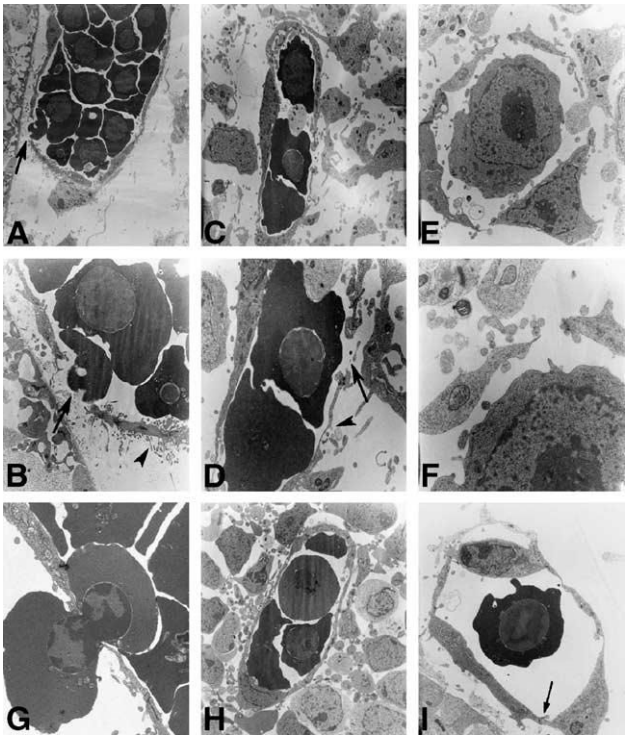

Fig. 5.

Hemorrhaging vessels display endothelial cell defects. Electron microscopy photomicrographs of ultra-thin frontal sections of heads from hemorrhaging E11.5 embryos (A–H) and wild type litter mate (I). A and B: low (A) and high magnification images (B) of vessel in the choroid plexus; arrow: gap in endothelial wall with extruding erythrocyte; arrowhead: abnormal, filopodia-like projections on endothelial cells. C and D: same animal as in A and B; arrow: break in endothelial wall; arrowhead: fenestration in endothelial cell. E and F: same animal as in A and B; note the large gaps between endothelial cells. G: small vessel from second hemorrhaging embryo; note extravasation of single erythrocyte. H: same animal as in A and B; small vessel embedded the neuronal tissue without endothelial cell defect. I: wild type littermate control, capillary from meningeal plexus with intact endothelium and intact cell junction (arrow). A total of 3 mutant embryos and 2 wild type littermates from 2 E11.5 litters were examined.

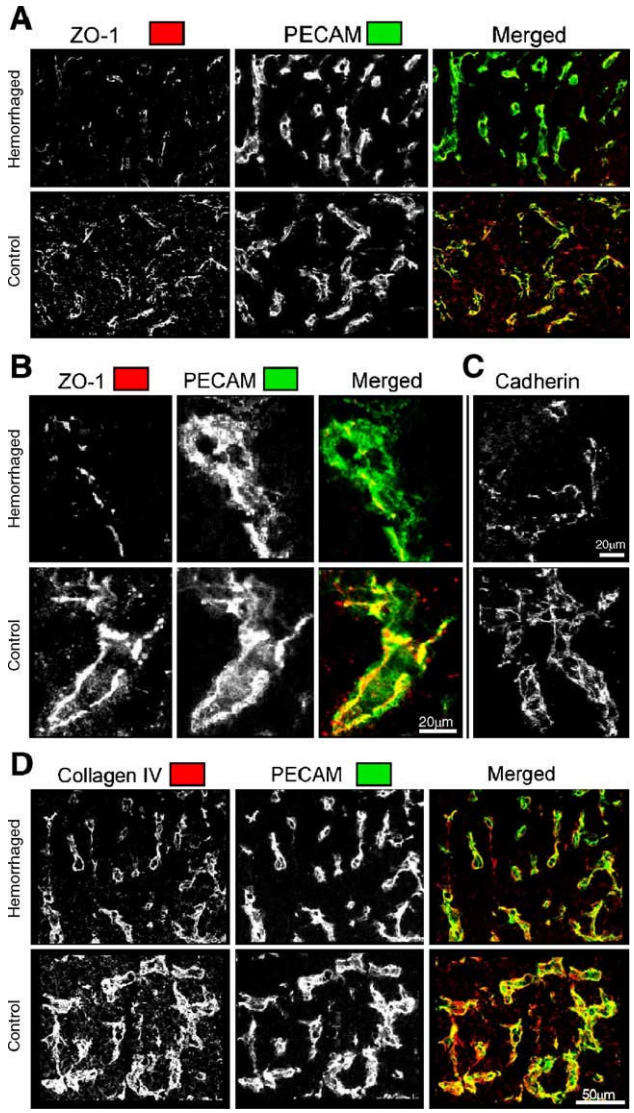

Fig. 6.

Mutant vessels display abnormal expression of cell junction and ECM proteins. Immunofluorescence studies and confocal microscopy of dorsal regions from hemorrhaging E11.5 embryos and wild type littermate controls. (A) Immunostaining with anti-ZO-1, anti-PECAM-1, and respective merged images at low magnification; yellow indicates co-localization. (B) High magnification from same section. Note the dramatically reduced and patchy pattern of anti-ZO-1 in mutant embryo. (C) High magnification image of vessels stained with anti-VE-cadherin. Note reduced and patchy expression. (D) Immunostaining with anti-Collagen IV, anti-PECAM-1, and respective merged images at low magnification; yellow indicates co-localization. Note the overall reduced pattern of anti-Collagen IV in mutant embryo. A total of 3 mutant embryos and 2 wild type littermates from 2 E11.5 litters were examined.

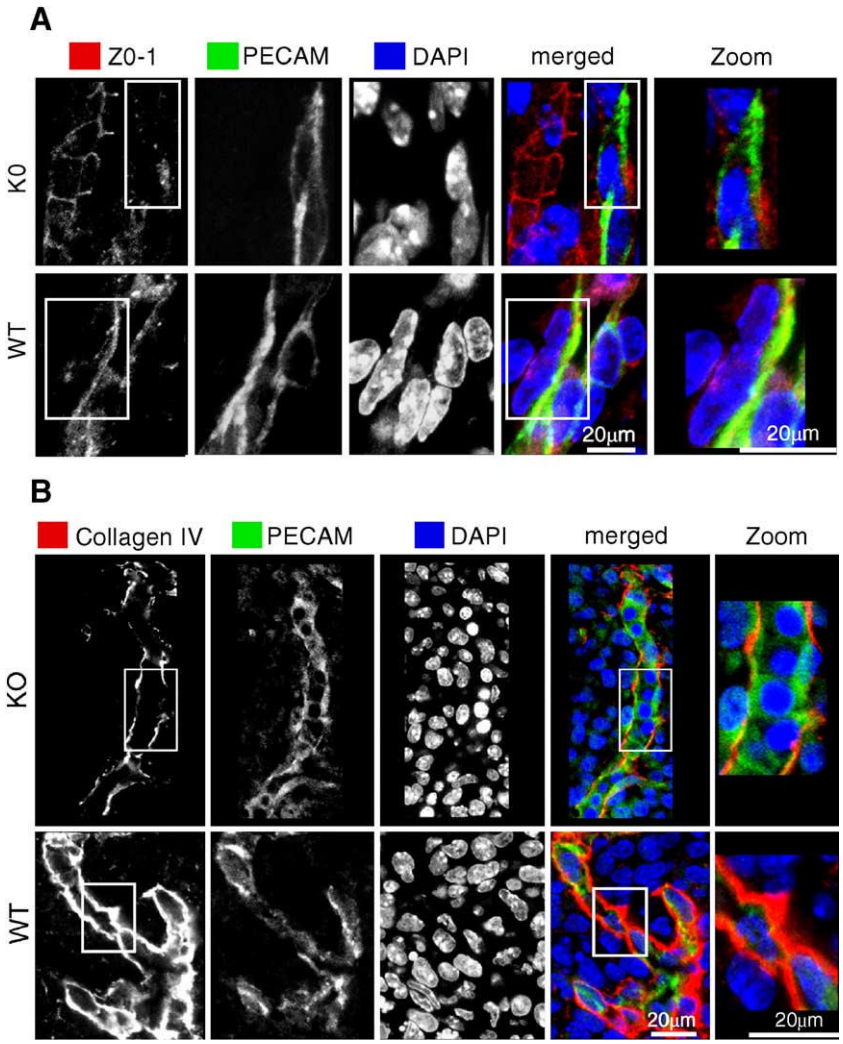

Fig. 7.

Vezf1$^{-/-}$ vessels are predisposed to loss of endothelial integrity. Immunofluorescence studies and confocal microscopy of dorsal regions from E10.5 *Vezf1*$^{-/-}$ embryos and wild type littermate controls. No signs of hemorrhaging were detected in these embryos. (A) Immunostaining with anti-ZO-1, anti-PECAM-1, respective merged images, and high magnification detail of boxed area; yellow indicates co-localization. Note that non-endothelial, PECAM-negative cells in the KO panel show continuous ZO-1 deposition. (B) Immunostaining with anti-Collagen IV, anti-PECAM-1, respective merged images, and high magnification detail of boxed area; yellow indicates co-localization. Spotty, discontinuous ZO-1 staining (A) and thinner layers and disjointed deposition of Collagen IV (B) were detected in *Vezf1*$^{-/-}$ vessels and capillaries in the absence of hemorrhaging or overt vascular abnormalities. Note that the overall pattern is similar to that detected in vessels of hemorrhaging E11.5 embryos (Fig. 6). Two E10.5 *Vezf1*$^{-/-}$ embryos and 2 wild type littermates were examined.

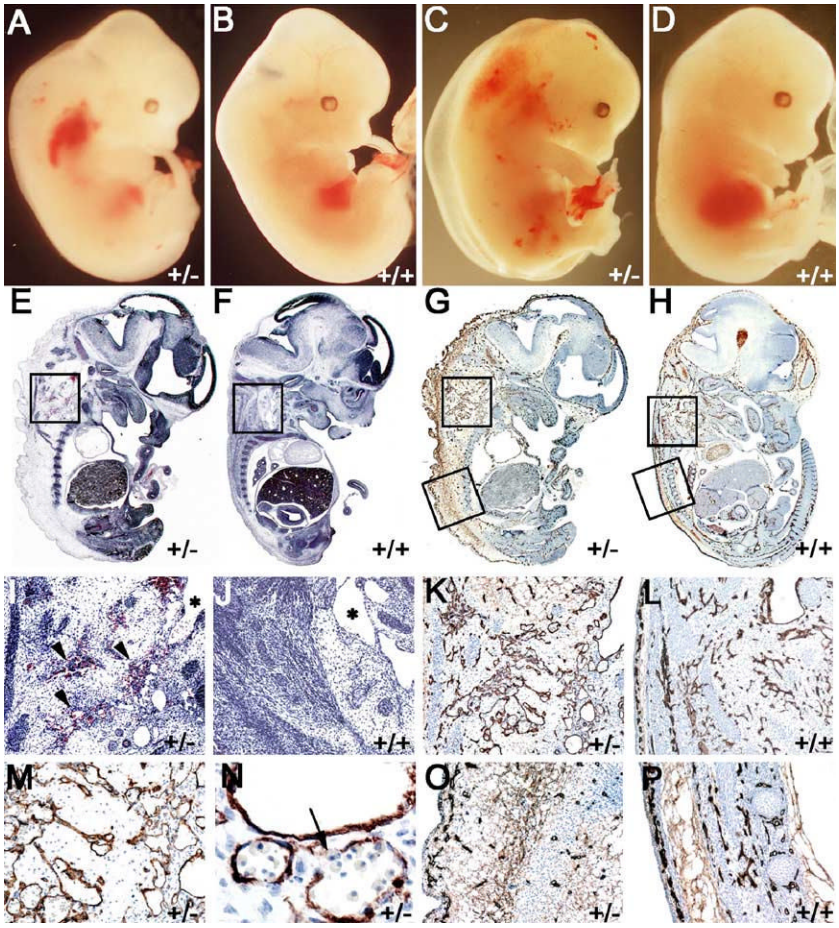

Fig. 8.

Hypervascularization, edema, and hemorrhaging in heterozygous Vezf1 embryos. (A–D) Photomicrographs of whole-mount E12.5 (A and B) and E13.5 (C and D) embryos. Hemorrhaging became apparent in the jugular region of a mutant E12.5 *Vezf1*$^{+/-}$ embryo (A). Affected E13.5 *Vezf1*$^{+/-}$ embryo (C) displayed severe edema and hemorrhaging in the back and neck. (B and D) Wild type controls. (E and F) H&E staining of parasagittal sections of E13.5 *Vezf1*$^{+/-}$ (E) and wild type control (F) embryos. Severe edema in the back region, hypervascularization, and hemorrhaging are visible in the jugular area of the heterozygous embryo (E). Boxed areas depict regions shown at higher magnification in panels I and J. (G and H) PECAM-1 staining of parasagittal sections close-by to those shown in (E and F). PECAM-1 staining outlines the embryonic vasculature and shows that hypervascularization is confined to the neck and back region of the mutant embryo (G). Boxed areas depict regions shown under higher magnification in panels K and O, and L and P, respectively. (I and J) High magnification images of the jugular region from embryos shown in E and F. Arrowheads: abnormal vessels in jugular region; *jugular sac. (K–N) High magnification photomicrographs of the jugular region of mutant *Vezf1*$^{+/-}$ embryo (K, M, N) and a wild type control (L) shown in G and H. Hypervascularization with abnormal vessel morphology and loose surrounding connective tissue is visible in the jugular region (K and M). Lesions in the endothelial wall of small vessels and erythrocytes leaking into the surrounding connective tissue (arrow) are detected in the neck region (N). (O and P) High magnification photomicrographs of the dorsal region of mutant *Vezf1*$^{+/-}$ embryo (O) and wild type control (P) shown in G and H. The heterozygous mutant embryo (O) displayed tissue swelling and masses of loose connective tissue.

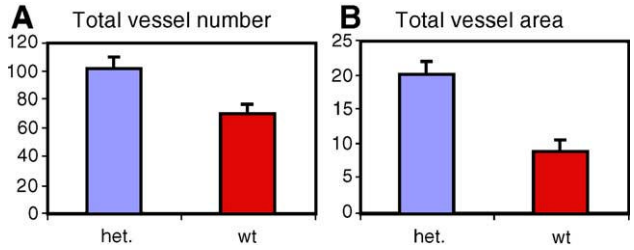

Fig. 9.

Quantitative morphometric analysis of the vasculature in the jugular region of heterozygous and wild type E13.5 embryos. (A) Total vessel number, (B) total vessel area. Three mutant *Vezf1*$^{+/-}$ and 3 wild type embryos were examined. Mutant *Vezf1*$^{+/-}$ embryos show increased vascularity in the jugular region, as measured by the extent of PECAM-1-positive structures. Bars and errors indicate mean and SD values.

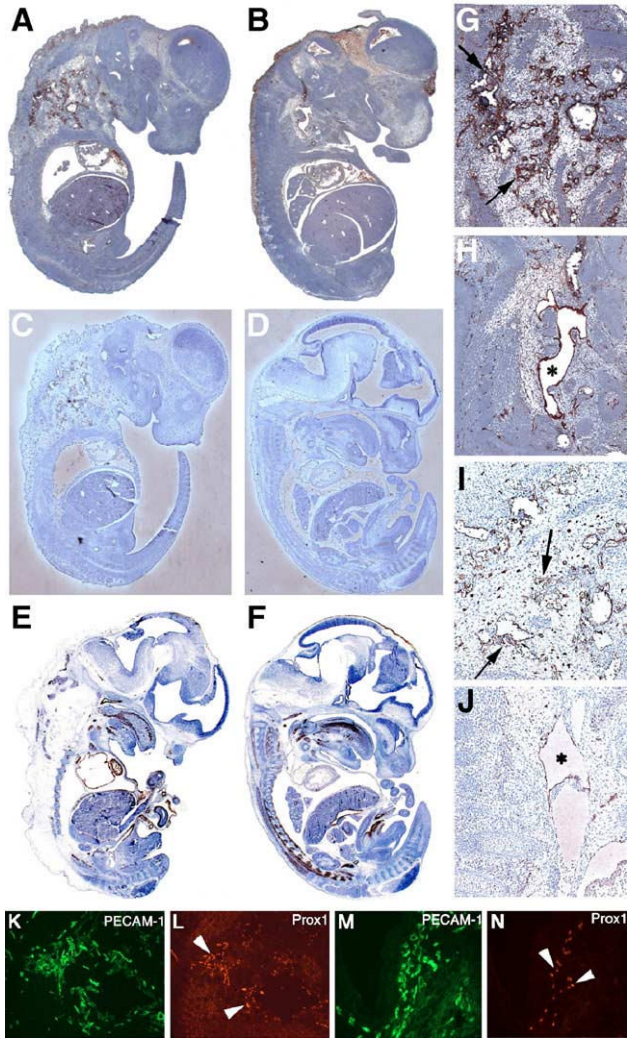

Fig. 10.

Lymphatic hypervascularization in heterozygous mutant E13.5 embryos. (A–F) Parasagittal sections of an E13.5 *Vezf1*$^{+/-}$ embryo (A, C, E) and wild type control embryo (B, D, F). Sections were immunostained for the lymphatic markers VEGFR-3 (A and B) and LYVE-1 (C and D), and for the VSMC marker SMa-actin (E and F). The hyperplastic vessels in the jugular region of heterozygous E13.5 embryos stain positive for the lymphatic markers VEGFR-3 (A) and LYVE-1 (C), but are negative for SMa-actin (E). (G and H) High magnification of the jugular region from images shown in (A and B). (I and J) High magnification of the jugular region from images shown in (C and D). Jugular sacs in wild type control are depicted by *. Examples of hyperplastic vessels in heterozygous embryos are depicted by arrows in G and I. (K–N) Cryostat sections from a mutant *Vezf1*$^{+/-}$ (K and L) embryo and a wild type littermate (M and N) were double immunostained for PECAM-1 (K and M) and Prox1 (L and N). Arrowheads depict Prox1-positive endothelial cells that appear disorganized in heterozygous (L) but not in wild type control embryos (N).

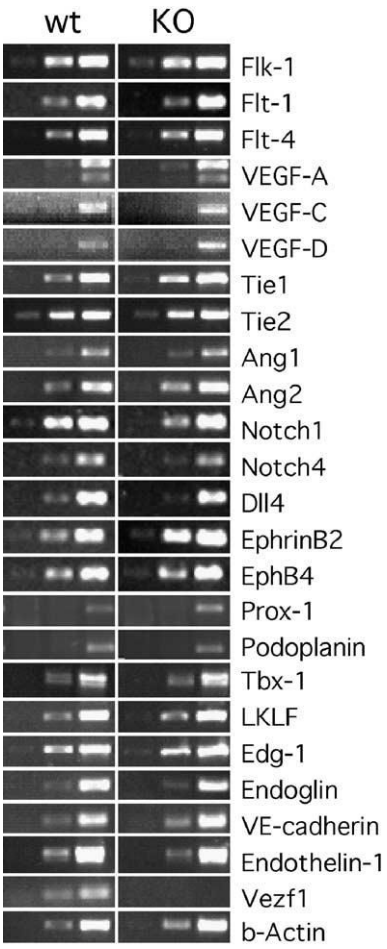

Fig. 11.

Gene expression analysis in *Vezf1*$^{-/-}$ embryos. Semi-quantitative RT-PCR (25, 30, and 35 cycles) using transcript-specific primers was performed on total RNA isolated from E10.5 *Vezf1*$^{-/-}$ and wild type embryos. Primer pairs specific for Vezf1 and b-actin transcripts were included in the analysis as controls, and to normalize for RNA amounts, respectively. Vezf1 transcripts are absent in *Vezf1*$^{-/-}$ embryos.

Table 1

Genotypes from *Vezf1*$^{+/-}$ × *Vezf1*$^{+/-}$ intercrosses in C57BL/6 background[a]

Development stage	No. of embryos	+/+	+/-[b]	-/-[b]	Frequency of -/- embryos (%)
E9.5	97	27	52	18 (8)	19
E10.5	47	14	28 (2)	5 (2)	11
E11.5	79	23	45 (2)	11 (5)	14
E12.5	79	23	46 (10)	10 (4)	13
E13.5	45	7	32 (7)	6 (2)	13
E14.5	13	5	7	1	8
E16.5	11	2	8	1 (1)	9
P0	21	9	13	0	0

[a] Embryos from *Vezf1*$^{+/-}$ × *Vezf1*$^{+/-}$ intercrosses (F5 to F10 backcross generation in the C57BL/6 background) were analyzed. Embryos from embryonic stages E9.5 to E16.5 were genotyped by performing PCR on genomic yolk sac DNA with primer pairs specific for the wild type and targeted allele. DNA from tail clips was used for genotyping of newborn pubs (P0).

[b] Numbers in parentheses represent embryos with vascular abnormalities and hemorrhaging.

Table 2

Genotype of progeny from heterozygous *Vezf1*$^{+/-}$ intercrosses in a mixed genetic background[a]

Development stage	No. of embryos/pups	+/+	+/-[b]	-/-[b]
E10.5	14	3	7	4
E11.5	14	3	6	5
E12.5	44	16	26 (2)	2 (2)
E13.5	10	3	7 (1)	0
E14.5	35	10	20	5 (1)
E15.5	12	2	9	1 (1)
E16.5	2	1	1	0
P0	53	15	30	8 (stillborn)
P21	46	16	30	0

[a] Heterozygous F1 (129/Sv × C57BL/6) males were bred with outbred CD-1 females, and offspring from F2 intercrosses were analyzed. Embryos from embryonic stages E10.5 to E16.5 were genotyped by performing PCR on genomic yolk sac DNA with primer pairs specific for the wild type and targeted allele. Newborn (P0) and 3-week-old offspring (P21) genotyped by performing PCR or Southern analysis on tail DNA.

[b] Numbers in parentheses represent embryos with vascular abnormalities and hemorrhaging.